nature catalysis

SUPPLEMENTARY INFORMATION

https://doi.org/10.1038/s41929-019-0277-8

In the format provided by the authors and unedited.

Intrinsically stable in situ generated electrocatalyst for long-term oxidation of acidic water at up to 80 °C

Manjunath Chatti[1,2], James L. Gardiner[1], Maxime Fournier[1,2], Bernt Johannessen[3], Tim Williams[4], Thomas R. Gengenbach[5], Narendra Pai[1], Cuong Nguyen[1], Douglas R. MacFarlane[1,2], Rosalie K. Hocking[6] and Alexandr N. Simonov[1,2]*

[1]School of Chemistry, Monash University, Clayton, Victoria, Australia. [2]ARC Centre of Excellence for Electromaterials Science, Monash University, Clayton, Victoria, Australia. [3]Australian Synchrotron, Clayton, Victoria, Australia. [4]Monash Centre for Electron Microscopy, Monash University, Clayton, Victoria, Australia. [5]Commonwealth Scientific and Industrial Research Organisation Manufacturing, Clayton, Victoria, Australia. [6]Department of Chemistry and Biotechnology, Swinburne University of Technology, Hawthorn, Victoria, Australia. *e-mail: alexandr.simonov@monash.edu

TABLE OF CONTENTS

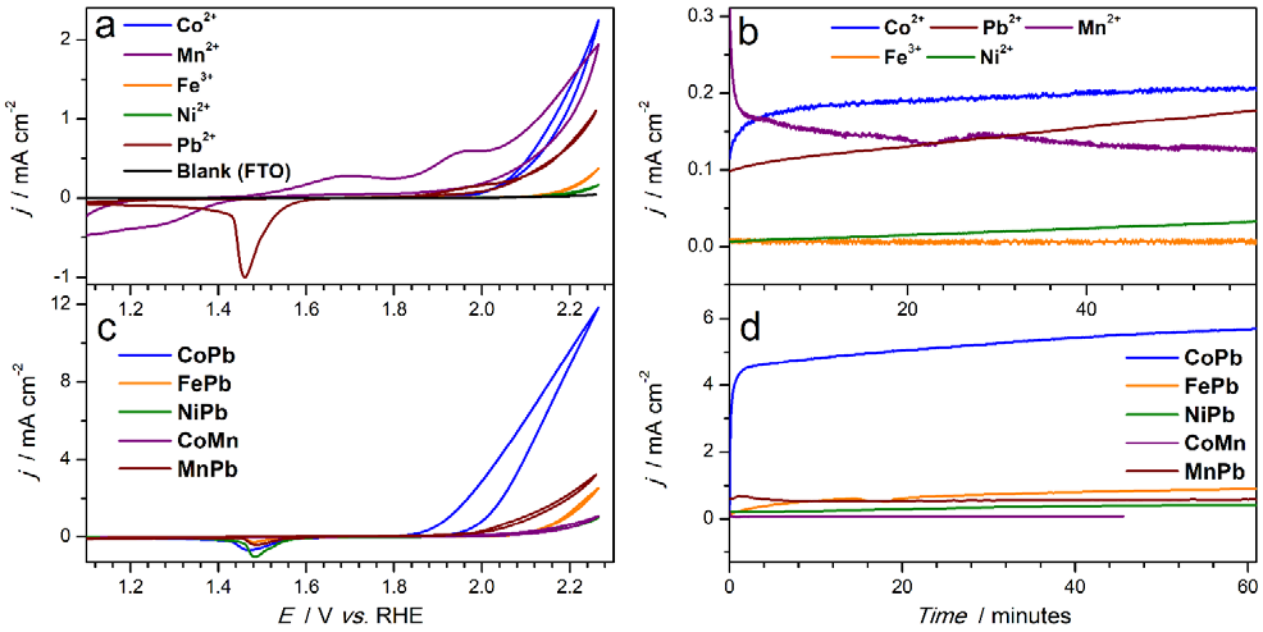

Supplementary Figure 1. (a, c) Cyclic voltammetric (scan rate 0.020 V s^{-1}) and (b, d) chronoamperometric (2.03 V *vs.* RHE; not corrected for ohmic losses) data obtained with a FTO electrode in contact with aqueous 0.1 M H_2SO_4 containing (a, b) 1 mM Co^{2+} (*blue*), Fe^{3+} (*orange*), Mn^{2+} (*purple*), Ni^{2+} (*green*) or Pb^{2+} (*brown*), or (c, d) 0.5 mM Co^{2+} + 0.5 mM Pb^{2+} (*blue*), 0.5 mM Fe^{3+} + 0.5 mM Pb^{2+} (*orange*), 0.5 Mm Ni^{2+} + 0.5 mM Pb^{2+} (*green*), 0.5 mM Co^{2+} + 0.5 mM Mn^{2+} (*purple*) or 0.5 mM Mn^{2+} + 0.5 mM Pb^{2+} (*brown*). In panels (a) and (c), quasi-stabilised (20^{th}) voltammetric cycles are shown. Currents are normalised to the geometric surface area of the electrodes; potentials are not corrected for ohmic losses.

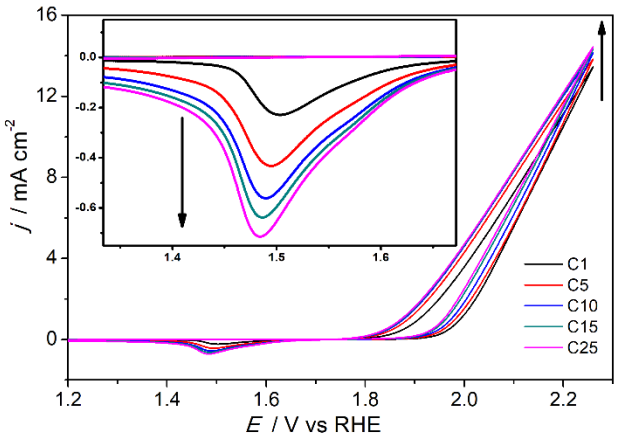

Supplementary Figure 2. Cyclic voltammograms (scan rate 0.020 V s^{-1}) recorded for a FTO electrode in contact with aqueous 0.1 M H_2SO_4 containing 5 mM Co^{2+} and 0.5 mM Pb^{2+}. Of 25 consecutive cycles, every 5th is shown. Inset shows the expanded plot of the PbO_2 reduction peak. Data are not corrected for ohmic losses; currents are normalised to the geometric surface area of the electrodes.

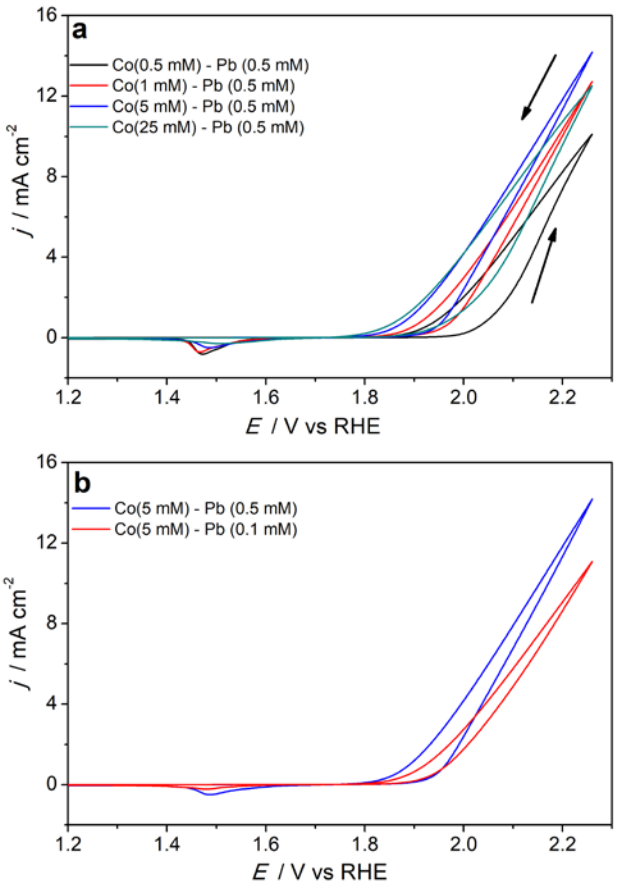

Supplementary Figure 3. Cyclic voltammograms (scan rate 0.020 V s^{-1}) obtained with a FTO electrode in contact with aqueous 0.1 M H_2SO_4 containing (a) 0.5 mM Pb^{2+} with 0.5 (*black*), 1 (*red*), 5 (*blue*) or 25 mM (*teal*) Co^{2+}, and (b) 5 mM Co^{2+} with 0.5 (*blue*) or 0.1 mM (*red*) Pb^{2+}. Quasi-stabilised (typically 20th) voltammetric cycles are shown. Currents are normalised to the geometric surface area of the electrodes; potentials are not corrected for ohmic losses.

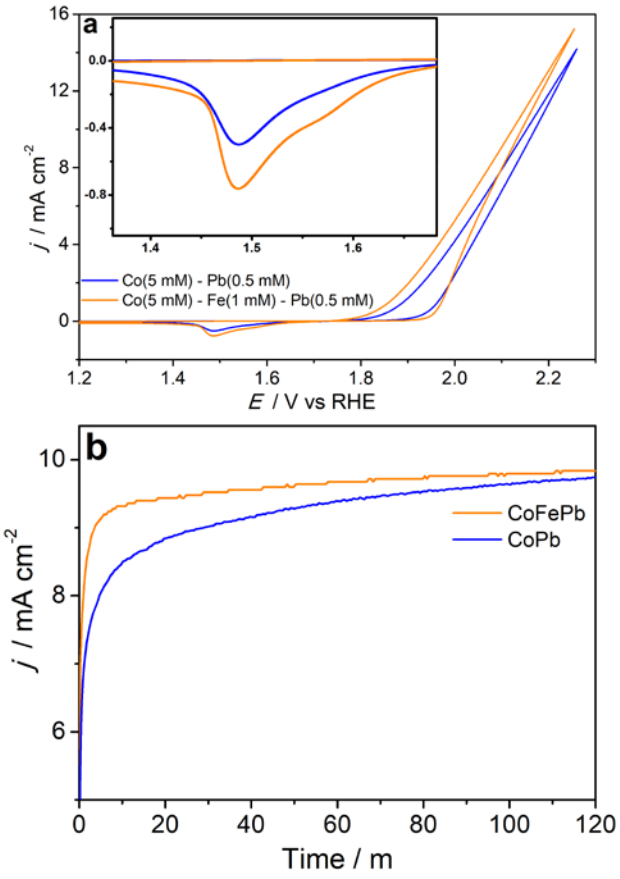

Supplementary Figure 4. (a) Cyclic voltammograms (scan rate 0.020 V s^{-1}) and (b) chronoamperograms (2.03 V vs. RHE; not corrected for iR_u drop) recorded with FTO electrodes in contact with aqueous 0.1 M H_2SO_4 containing 5 mM Co^{2+} + 1 mM Fe^{3+} + 0.5 mM Pb^{2+} (*orange*) or 5 mM Co^{2+} + 0.5 mM Pb^{2+} (*blue*). In panel (a), quasi-stabilised (20^{th}) voltammetric cycles are shown. Currents are normalised to the geometric surface area of the electrodes; potentials are not corrected for ohmic losses.

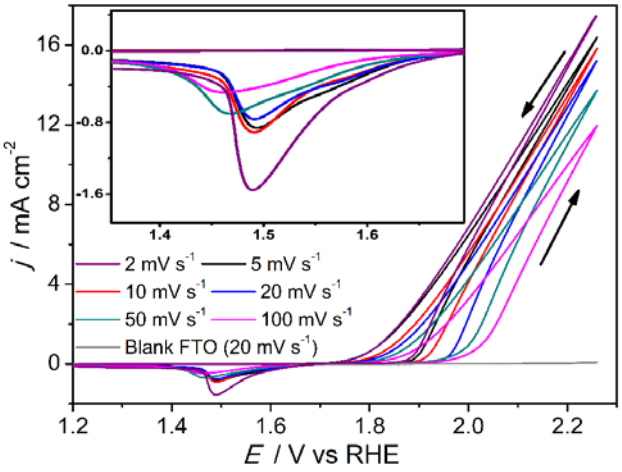

Supplementary Figure 5. Cyclic voltammograms obtained with a FTO electrode and aqueous 0.1 M H_2SO_4 containing 5 mM Co^{2+} + 1 mM Fe^{3+} + 0.5 mM Pb^{2+} at different scan rates: 0.002 (*purple*), 0.005 (*black*), 0.010 (*red*), 0.020 (*blue*), 0.050 (*teal*) and 0.100 V s^{-1} (*magenta*). Data obtained with pure 0.1 M H_2SO_4 at 0.02 V s^{-1} are shown as *grey* curve. Quasi-stabilised (typically 20th) voltammetric cycles are shown. Currents are normalised to the geometric surface area of the electrodes; potentials are not corrected for iR_u drop.

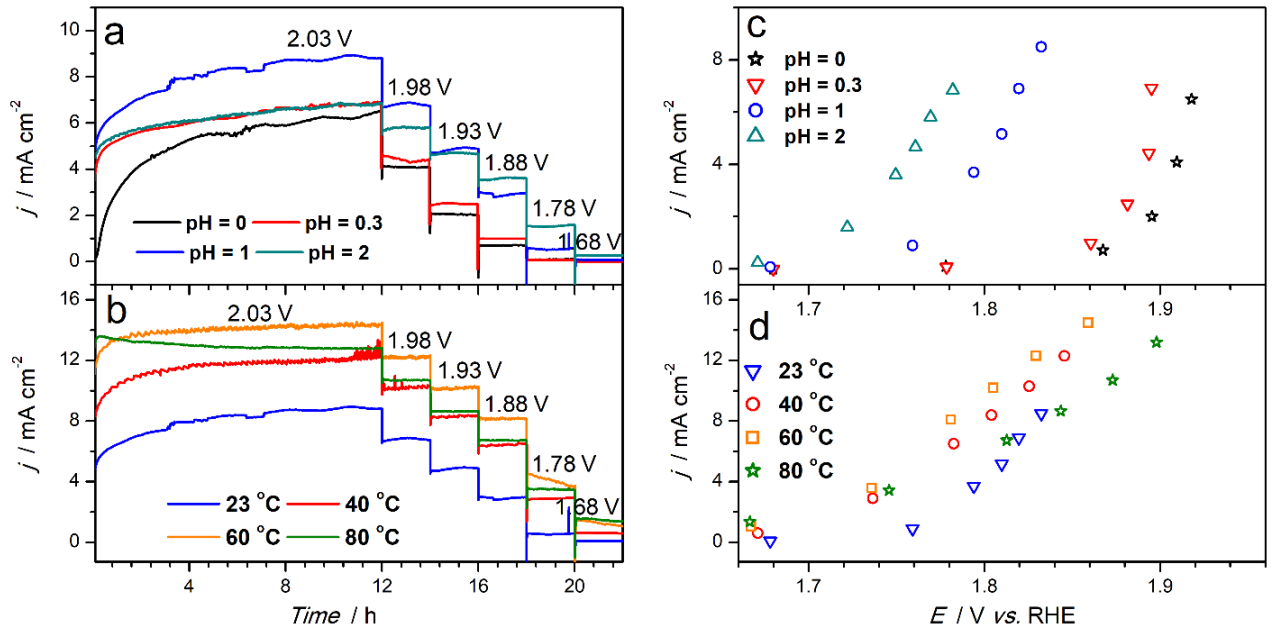

Supplementary Figure 6. Potentiostatic oxidation of H_2SO_4 solutions containing 5 mM Co^{2+} + 1 mM Fe^{3+} + 0.5 mM Pb^{2+} using FTO electrodes under different conditions: (a) T = 23 °C, pH = 2.00 (*teal*), 1.00 (*blue*), 0.30 (*red*) and 0.00 (*black*); (b) pH = 1.00, T = 23 (*blue*), 40 (*red*), 60 (*orange*) and 80 °C (*green*). Quasi-steady state current densities derived from the chronoamperograms at different (c) pH and (d) temperature as a function of potential. Currents are normalised to the actual geometric surface area of the electrodes. Potentials are referred to RHE and are not corrected for ohmic losses.

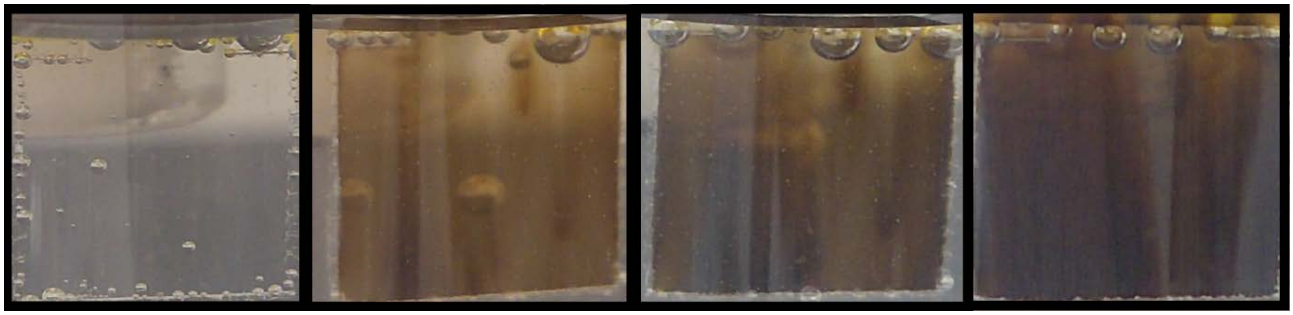

Supplementary Figure 7. Progressive photographs of FTO electrode taken over (from left to right) 0, 2, 6 and 24 hours during galvanostatic oxidation (10 mA cm^{-2}) of 0.1 M H_2SO_4 containing 5 mM Co^{2+}, 1 mM Fe^{3+} and 0.5 mM Pb^{2+} at 23 °C.

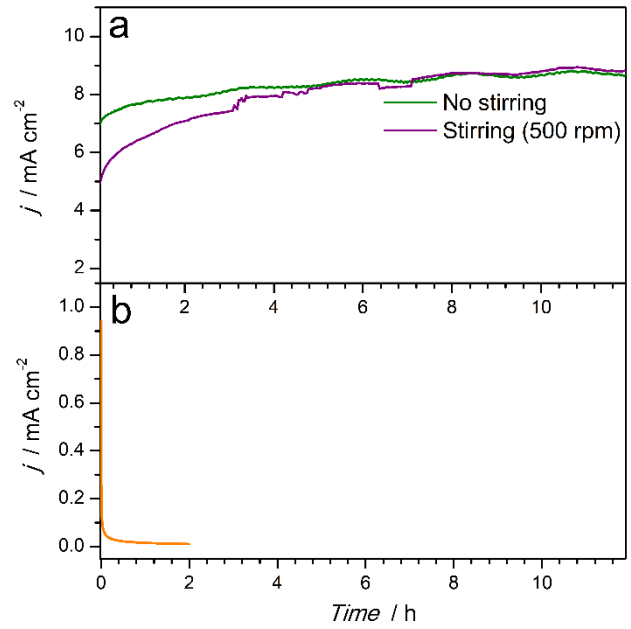

Supplementary Figure 8. (a) Effect of stirring (magnetic stirrer at 500 rpm) on the chronoamperometric oxidation of 0.1 M H_2SO_4 solution containing 5 mM Co^{2+}, 1 mM Fe^{3+} and 0.5 mM Pb^{2+} using FTO electrodes. (b) Simulated chronoamperograms for the diffusion-controlled oxidation of 5 mM $Co^{2+/3+}$ (diffusion coefficient, D = 0.73 × 10^{-5} cm^2 s^{-1})[S1], 1 mM $Fe^{3+/4+}$ (D = 0.60 × 10^{-5} cm^2 s^{-1})[S1] and 0.5 mM $Pb^{2+/4+}$ (D = 0.95 × 10^{-5} cm^2 s^{-1})[S1] at a planar electrode. Currents are normalised to the geometric surface area.

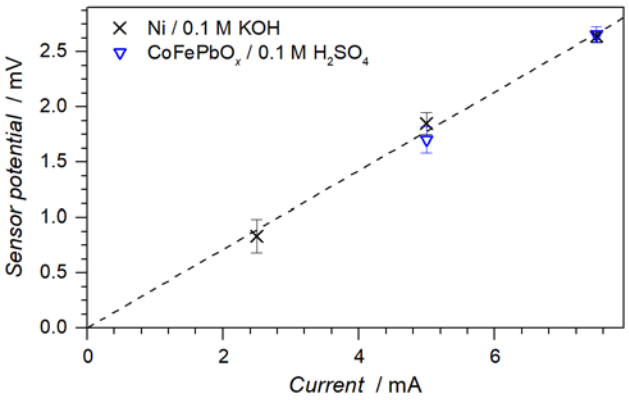

Supplementary Figure 9. Stabilised response of an oxygen sensor recorded at defined currents during the electrooxidation of aqueous 0.1 M H_2SO_4 solution containing 5 mM Co^{2+} + 1 mM Fe^{3+} + 0.5 mM Pb^{2+} using an FTO electrode (*blue*), and of aqueous 0.1 M KOH using low surface area Ni wire (*black*). Data points and error bars show average values and one standard deviation for three measurements. Line is linear fit to the *black* data.

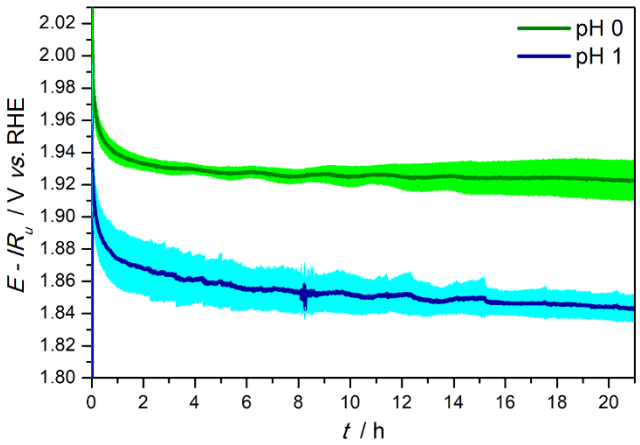

Supplementary Figure 10. Galvanostatic oxidation of aqueous 0.1 M (*blue* and *turquoise*) and 1 M (*green* and *light green*) H_2SO_4 solutions containing 5 mM Co^{2+}, 1 mM Fe^{3+} and 0.5 mM Pb^{2+} at 10 mA cm^{-2} and 23 °C using FTO electrodes. Data are corrected for ohmic losses. Curves show average values and shadings show one standard deviation calculated for three independent electrodes.

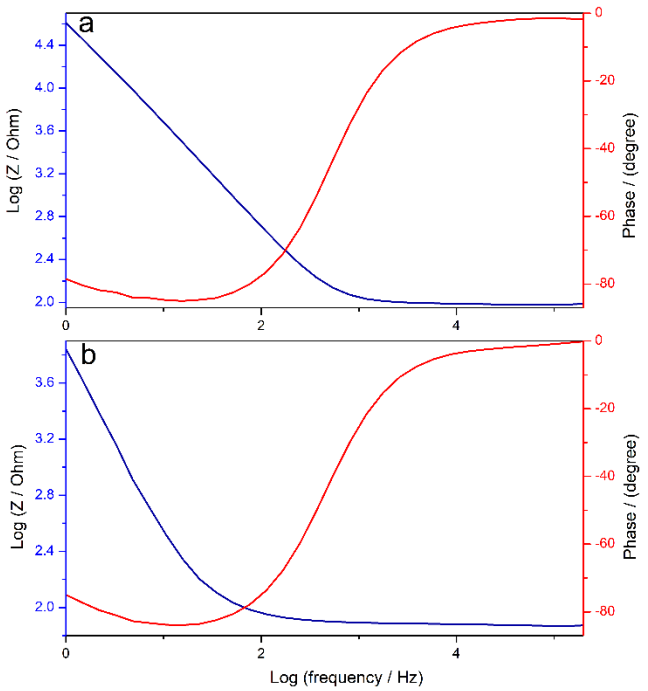

Supplementary Figure 11. Electrochemical impedance spectra measured with FTO electrodes in contact with H_2SO_4 solutions containing 5 mM Co^{2+}, 1 mM Fe^{3+} and 0.5 mM Pb^{2+} at open circuit potential under different conditions: T = 23 °C and pH = (a) 1.0 or (b) 0.0.

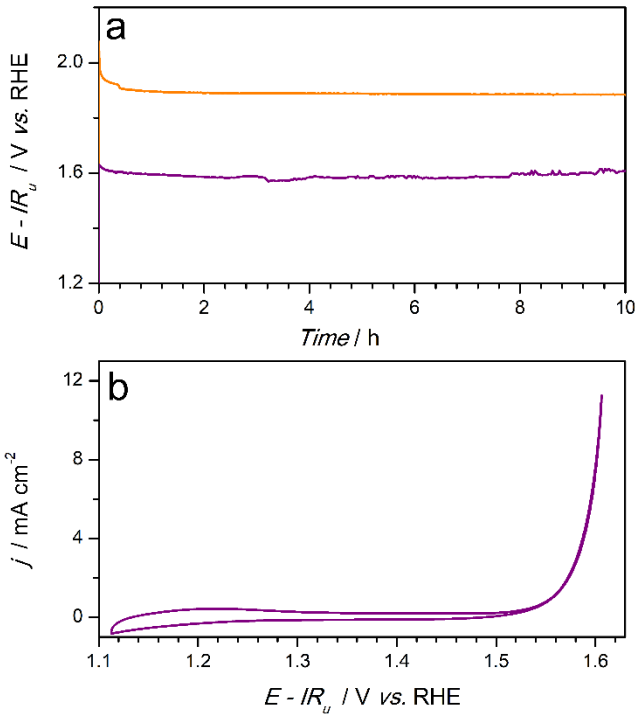

Supplementary Figure 12. (a) Galvanostatic oxidation (10 mA cm^{-2}) of aqueous 1 M H_2SO_4 containing 5 mM Co^{2+}, 1 mM Fe^{3+} and 0.5 mM Pb^{2+} with a FTO electrode (*orange*), and of pure aqueous 1 M KOH in the absence of any metal ions in the solution using the same electrode (*purple*). Potentials are corrected for ohmic losses. (b) Cyclic voltammetry (v = 0.005 V s^{-1}) of the $CoFePbO_x$/FTO electrode used in panel (a) in pure aqueous 1 M KOH. All measurements were at 23 °C.

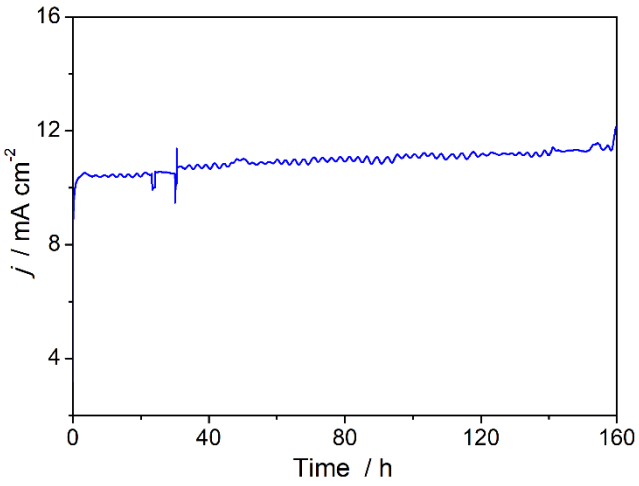

Supplementary Figure 13. Long-term potentiostatic oxidation of aqueous 0.1 M H_2SO_4 containing 5 mM Co^{2+}, 1 mM Fe^{3+} and 0.5 mM Pb^{2+} using an FTO electrode at 23 °C and at an applied potential of 2.03 V *vs.* RHE (not corrected for iR_u drop).

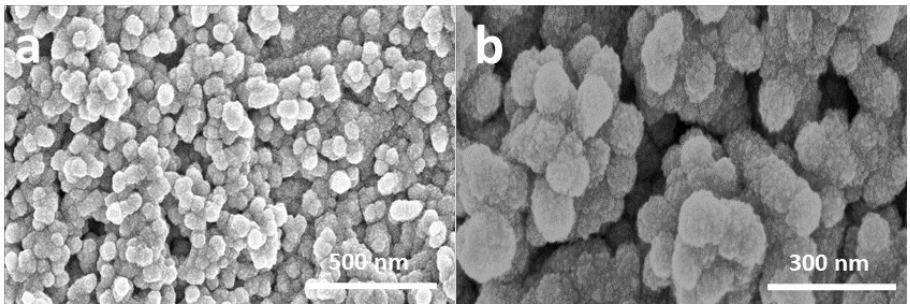

Supplementary Figure 14. (a, b) SEM images of the $CoFePbO_x$ catalyst generated on the FTO electrode at pH 0 and 23 °C. Electrodeposition was performed in a 1 M H_2SO_4 solution containing 5 mM Co^{2+}, 1 mM Fe^{3+} and 0.5 mM Pb^{2+} at an applied current density of 10 mA cm^{-2} for 12 h.

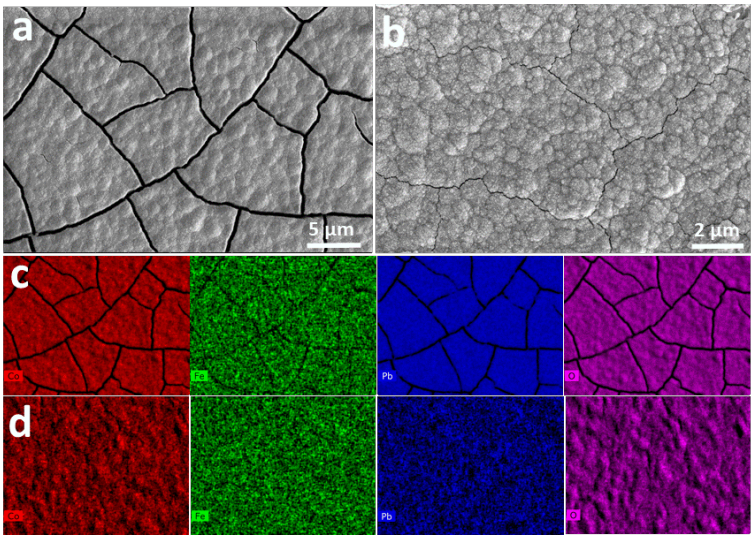

Supplementary Figure 15. (a, b) SEM images and (c, d) corresponding elemental maps derived from EDX analysis of the $CoFePbO_x$ catalysts generated on FTO electrodes at (a, c) 23 and (b, d) 60 °C. Electrodeposition was performed in 0.1 M H_2SO_4 solutions containing Co^{2+} (5 mM), Fe^{3+} (1 mM) and Pb^{2+} (0.5 mM) at an applied potential of 2.03 V *vs.* RHE (not corrected for iR_u losses) for 12 h. The nature of the cracks in the catalyst layers is not established at this stage; however, it is highly probable that those are formed upon drying and the accompanying uncontrollable contraction of the materials prior to the microscopic analysis.

Supplementary Table 1. Composition of catalyst films produced potentiostatically on FTO under different conditions[a] as determined by different techniques.

Technique	Co : Fe : Pb atomic ratio (%)		
	pH 1, 23 °C	pH 0, 23 °C	pH 1, 60 or 80 °C
EDX/SEM mapping	12 : 2 : 86	6 : 1 : 93	10 : 8 : 82 (60 °C)
ICP-OES	18 : 1 : 81	6 : 2 : 92	14 : 4 : 82 (80 °C)
XPS (surface)	25 : 0 : 75 [b]	11 : 0 : 89 [b]	22 : 0 : 78 [b] (80 °C)
XPS (bulk) [b]	35 : 0 : 65	not analysed	not analysed

[a] Other conditions: quiescent solutions with 5 mM Co^{2+} + 1 mM Fe^{3+} + 0.5 mM Pb^{2+}; deposition potential 2.03 V *vs.* RHE (not corrected for iR_u drop); deposition time 12 h. [b] Intensity of the Fe 2p signal was at the noise level. [c] After Ar etching for *ca* 5 min.

Supplementary Table 2. Temporal evolution of the composition and thickness of catalyst films[a] produced potentiostatically on FTO at 23 °C and pH 1.[b]

Deposition time (hours)	Co : Fe : Pb atomic ratio (%)	Thickness (μm)
2	17 : 1 : 82	<0.05
6	15 : 1 : 84	0.2
12	13 : 2 : 85	1
24	17 : 2 : 81	2
120	15 : 2 : 83	2

[a] Derived from SEM/EDX analysis. [b] Other conditions: quiescent solutions with 5 mM Co^{2+} + 1 mM Fe^{3+} + 0.5 mM Pb^{2+}; deposition potential 2.03 V *vs.* RHE (not corrected for iR_u drop).

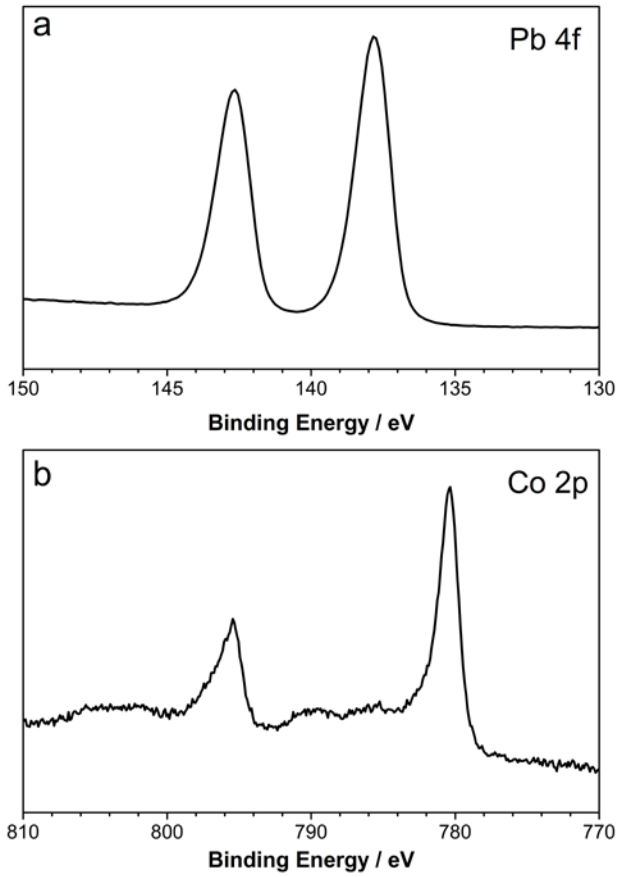

Supplementary Figure 16. (a) Pb 4f and (b) Co 2p XP spectra of the $CoFePbO_x$ electrocatalyst electrodeposited onto FTO in aqueous 0.1 M H_2SO_4 containing 5 mM Co^{2+}, 1 mM Fe^{3+} and 0.5 mM Pb^{2+} at 2.03 V *vs.* RHE (not corrected for iR_u drop) and 23 °C for 12 h.

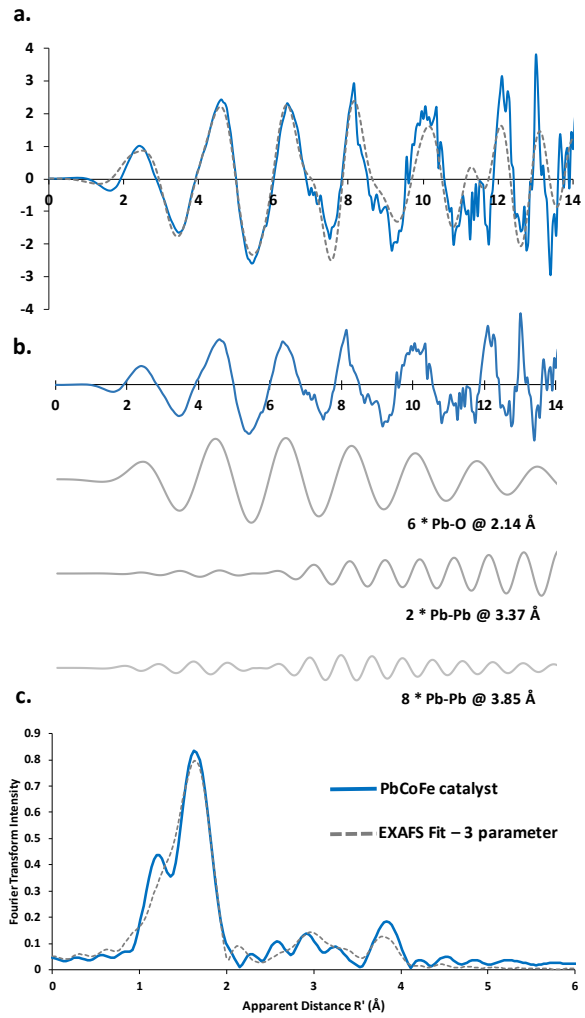

Supplementary Figure 17. Experimental (*blue*) and modelled (*grey*) Pb L_3-edge EXAFS data for the $CoFePbO_x$ catalyst (deposited during 12 h at 23 °C and at a non IR_u-corrected potential of 2.03 V in 0.1 M H_2SO_4 containing 5 mM Co^{2+} + 1 mM Fe^{3+} + 0.5 mM Pb^{2+}): (a) EXAFS, (b) three parameter split of the EXAFS fit, and (c) Fourier transformed EXAFS. Modelled data are based on three component fit with tabulated crystal structure parameters for β-PbO_2 (PDF 00-041-1492).

Supplementary Table 3. Parameters used for the simulation of the Pb L_3-edge EXAFS based on three parameter fit model using crystal structure data.

	N [a]	S02 [b]	σ^2 / Å^2 [c]	E0 [d]	*R* / Å [e]	*R*(crystal str) / Å [f]
Pb-O	6	0.467	0.00504	-3.39	2.145	2.162
Pb-Pb	2	0.467	0.00340	-3.39	3.370	3.388
Pb-Pb	8	0.467	0.00135	-3.39	3.852	3.893

[a] Coordination number; [b] Amplitude reduction parameter; [c] Debye-Waller parameter; [d] E0 parameter; [e] Interatomic distance; [f] Reference crystal structure data for β-PbO_2.

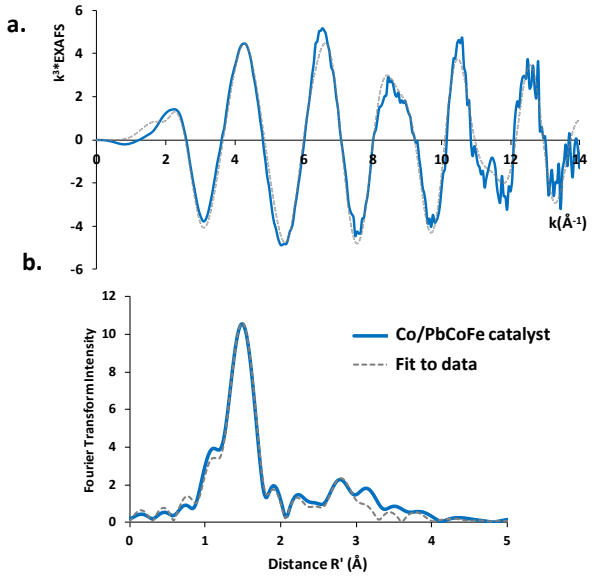

Supplementary Figure 18. Experimental (*blue*) and modelled (*grey*) Co K-edge EXAFS data for the $CoFePbO_x$ catalyst (deposited during 12 h at 23 °C and at a non IR_u-corrected potential of 2.03 V in 0.1 M H_2SO_4 containing 5 mM Co^{2+} + 1 mM Fe^{3+} + 0.5 mM Pb^{2+}): (a) EXAFS, (b) three parameter split of the EXAFS fit, and (c) Fourier transformed EXAFS. Modelled data are based on three component fit with tabulated crystal structure parameters for β-PbO_2 (PDF 00-041-1492).

Supplementary Table 4. Parameters used in the Co K-edge EXAFS simulation based on three parameter fit model using crystal structure data.

	N [a]	S02 [b]	σ^2 / Å² [c]	E0 [d]	*R* / Å [e]	*R* (crystal str) / Å [f]
Co-O	6	0.507	0.00266	-3.892	1.91	2.162
Co-Pb	2	0.507	0.00530	-3.892	2.86	3.388
Co-Pb	8	0.507	0.02465	-3.892	3.876	3.893
Co-O	4	0.507	0.04974	-3.892	3.409	3.75
Co-O-Pb	16	0.507	0.20284	-3.892	4.107	4.10

[a] Coordination number; [b] Amplitude reduction parameter; [c] Debye-Waller parameter; [d] E0 parameter; [e] Interatomic distance; [f] Reference crystal structure data for β-PbO_2.

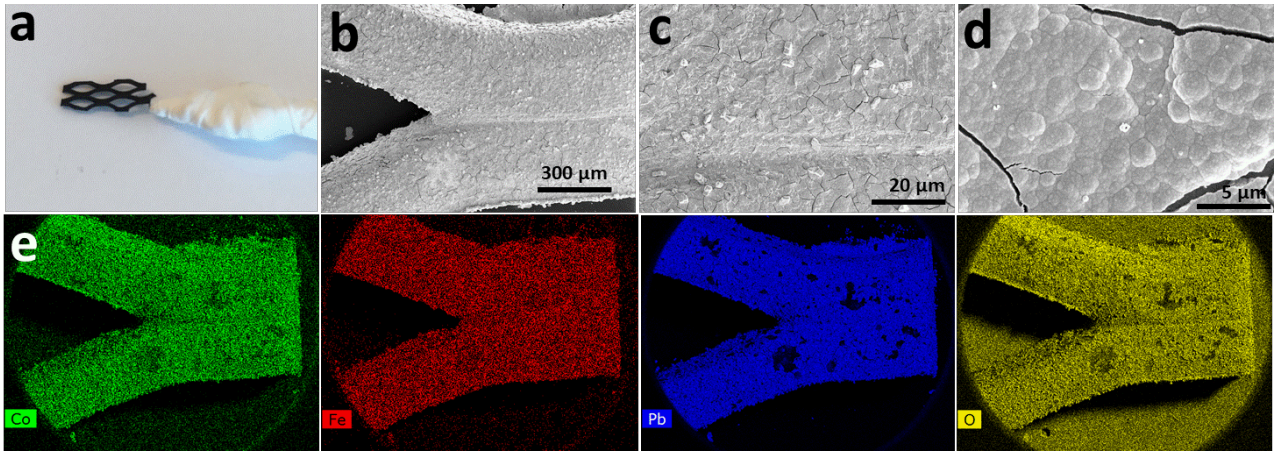

Supplementary Figure 19. (a) Photograph, (b-d) SEM images and (d) elemental maps derived from EDX analysis of a Pt/Ti electrode modified with a $CoFePbO_x$ catalyst at 23 °C. Electrodeposition was performed in aqueous 0.1 M H_2SO_4 containing 5 mM Co^{2+}, 1 mM Fe^{3+} and 0.5 mM Pb^{2+} at an applied potential of 2.03 V *vs.* RHE (not corrected for ohmic losses) for 12 h.

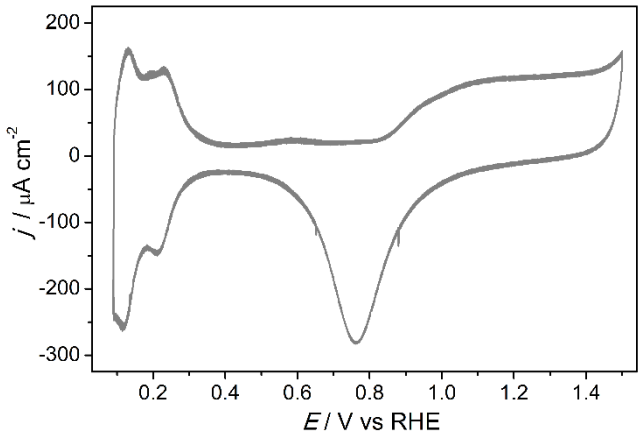

Supplementary Figure 20. Stabilised cyclic voltammetry (scan rate, $v = 0.020$ V s^{-1}) of a Pt/Ti electrode in Ar-saturated aqueous 0.1 M H_2SO_4. Currents are normalised to the geometric surface area of the electrode; potentials are not corrected for iR_u drop.

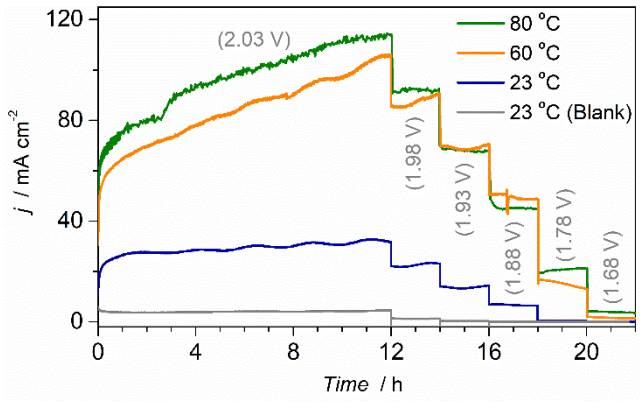

Supplementary Figure 21. Potentiostatic oxidation of 0.1 M H_2SO_4 containing 5 mM Co^{2+}, 1 mM Fe^{3+} and 0.5 mM Pb^{2+} using Pt/Ti electrodes at different temperature: 23 (*blue*), 60 (*orange*) and 80 °C (*green*). *Grey* curve shows data obtained with pure 0.1 M H_2SO_4 solution at 23 °C. Currents are normalised to the geometric surface area of the electrodes. Potentials on the RHE scale shown in brackets are not corrected for iR_u losses and are calculated for the initial situation where pH = 1 (see further discussion in main text).

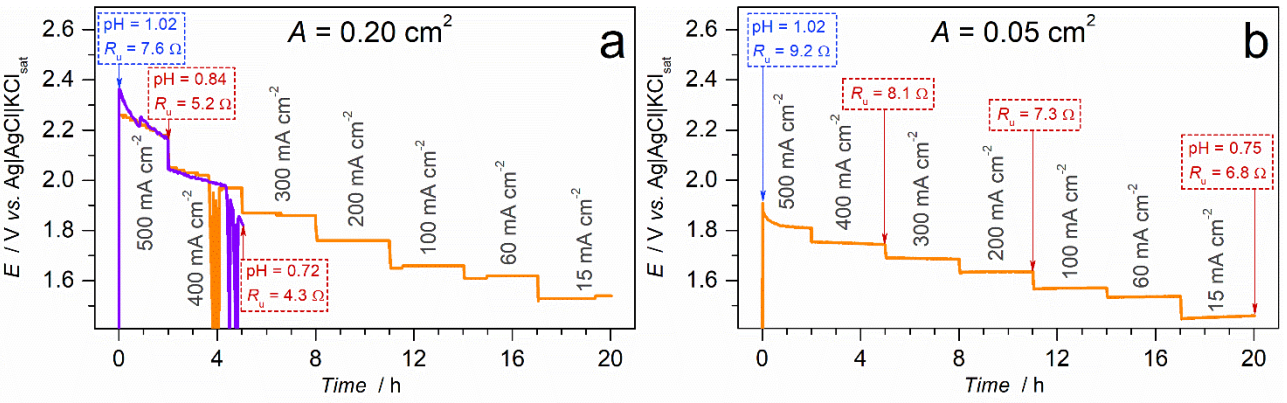

Supplementary Figure 22. Galvanostatic oxidation of 0.1 M H_2SO_4 containing 5 mM Co^{2+}, 1 mM Fe^{3+} and 0.5 mM Pb^{2+} at 60 °C using Pt/Ti electrodes with geometric area of (a) 0.20 and (b) 0.05 cm^2. Potentials are reported *vs.* Ag|AgCl|$KCl_{sat.}$ with no iR_u correction due to the pH and R_u changes during the measurement. In panel (a), *orange* and *purple* curves show data for two independent experiments. Dashed boxes report pH in the working electrode compartment and the measured R_u values at different stages of the experiments (for *purple* data in panel (a)). Drops in the potential in panel (a) between 3.5 and 5 h are associated with a very high resistance through the glass frit between working and auxiliary compartments developing due to the build-up of the concentration gradient of the supporting electrolyte (H^+ and HSO_4^-) within the frit. This very high resistance requires the auxiliary electrode to operate at potentials more negative than -20 V, which is beyond the capacity of the potentiostat employed herein. These effects do not appear when using the smaller electrode in panel (b) that generates 4-fold lower absolute current/charge and therefore a less significant pH gradient.

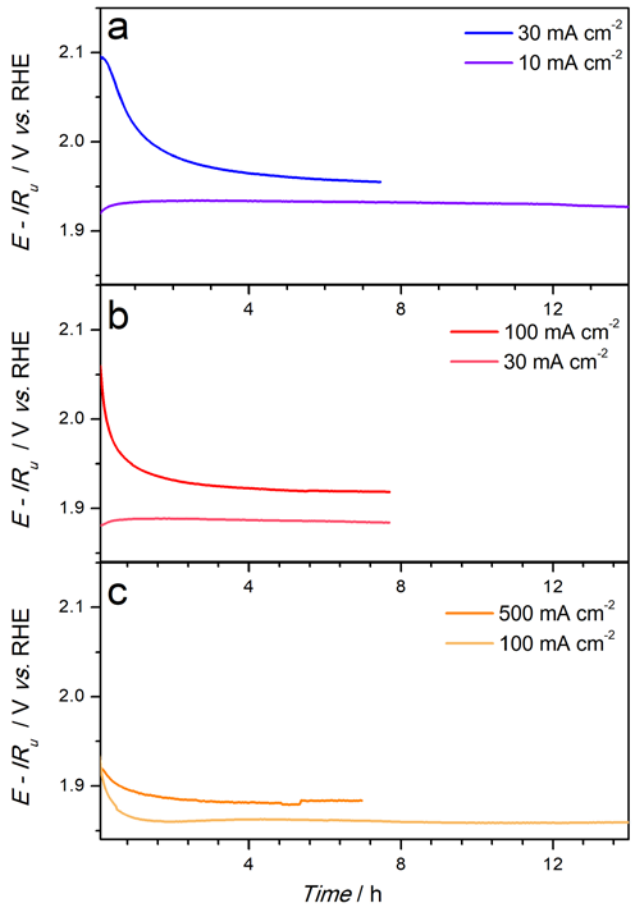

Supplementary Figure 23. Galvanostatic oxidation of aqueous 1 M H_2SO_4 containing 5 mM Co^{2+}, 1 mM Fe^{3+} and 0.5 mM Pb^{2+} at (a) 23, (b) 40 and (c) 60 °C using Pt/Ti electrodes. Potentials are corrected for IR_u losses.

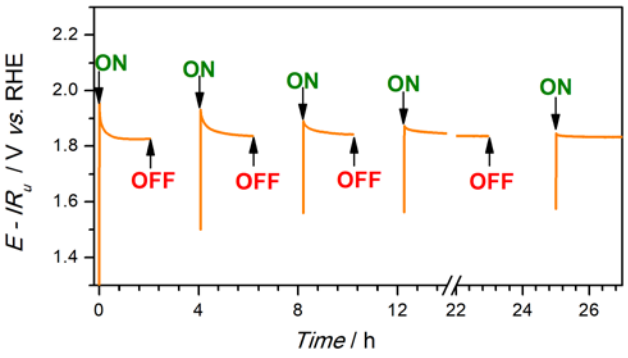

Supplementary Figure 24. Galvanostatic oxidation (operating current density 100 mA cm^{-2}) of aqueous 1 M H_2SO_4 containing 5 mM Co^{2+}, 1 mM Fe^{3+} and 0.5 mM Pb^{2+} at 60 °C using Pt/Ti electrodes in an interrupted regime (see "ON" and "OFF" labels in figure). Potentials are corrected for IR_u losses.

Supplementary Table 5. Composition of catalyst films produced on Pt/Ti mesh electrodes under different galvanostatic conditions[a] as determined by EDX and ICP-OES.

Technique	Co : Fe : Pb atomic ratio (%)		
	15 mA cm^{-2}	60 mA cm^{-2}	100 mA cm^{-2}
EDX/SEM mapping	11 : 2 : 87	11 : 2 : 87	7 : 1 : 92
ICP-OES	16 : 2 : 82	16 : 1 : 83	12 : 2 : 86

[a] Other conditions: quiescent 5 mM Co^{2+} + 1 mM Fe^{3+} + 0.5 mM Pb^{2+} in 0.1 M H_2SO_4, 60 °C, 12 h.

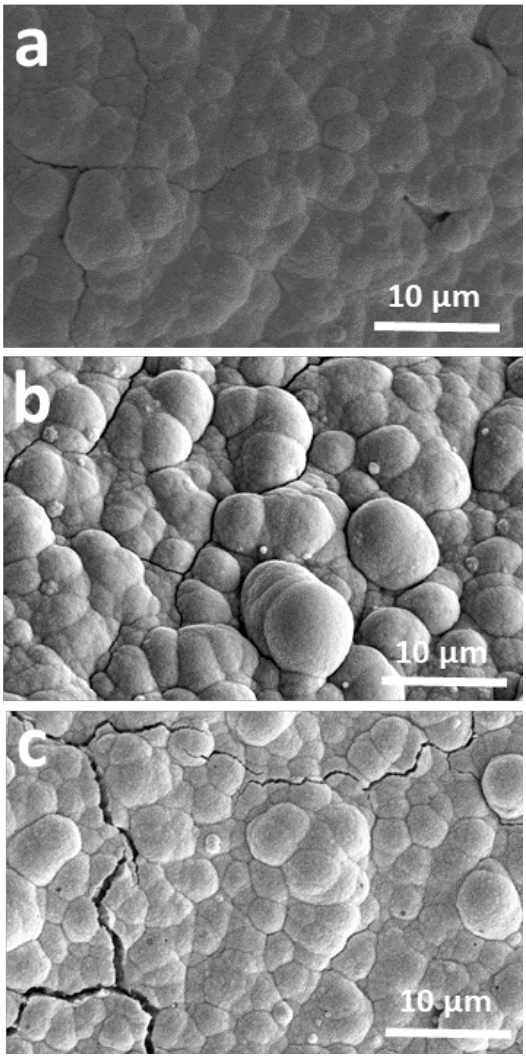

Supplementary Figure 25. SEM images of the $CoFePbO_x$ catalysts generated on Pt/Ti electrodes at 60 °C at an applied current density of (a) 15 mA cm^{-2}; (b) 60 mA cm^{-2} and (c) 100 mA cm^{-2} for 12 h. Electrodeposition was performed in stirred aqueous 0.1 M H_2SO_4 containing 5 mM Co^{2+}, 1 mM Fe^{3+} and 0.5 mM Pb^{2+}.

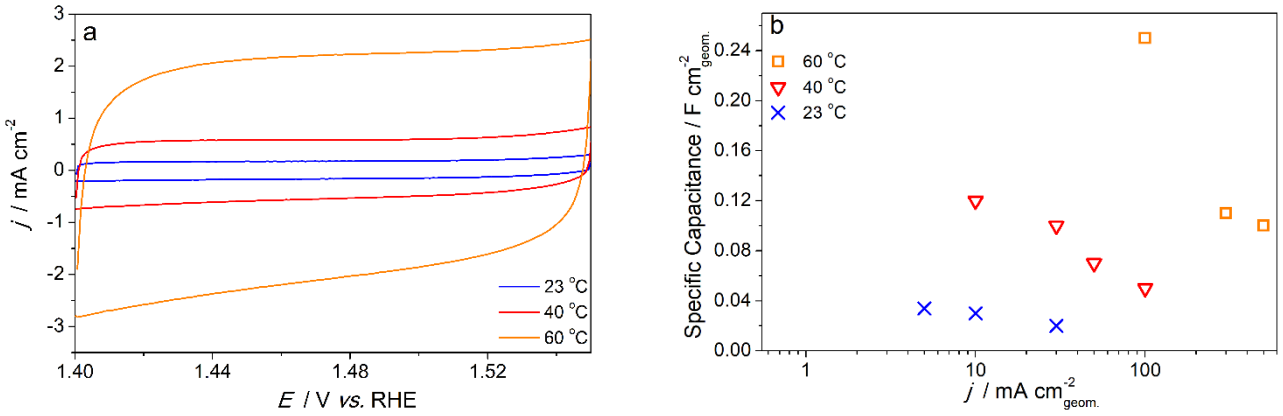

Supplementary Figure 26. (a) Cyclic voltammograms (v = 0.02 V s^{-1}) in air-saturated 1 M KOH for $CoFePbO_x$ catalysts deposited on Pt/Ti electrodes at 60 °C and 300 mA cm^{-2} (*orange*), 40 °C and 50 mA cm^{-2} (*red*), and 23 °C and 30 mA cm^{-2} (*blue*). Currents are normalised to the geometric surface area; potentials are not corrected for ohmic losses. (b) Specific capacitance of $CoFePbO_x$ catalysts electrodeposited on Pt/Ti electrodes at 60 (*orange*), 40 (*red*) and 23 °C (*blue*) as a function of the current density. All samples were obtained with 1 M H_2SO_4 containing 5 mM Co^{2+}, 1 mM Fe^{3+} and 0.5 mM Pb^{2+}.

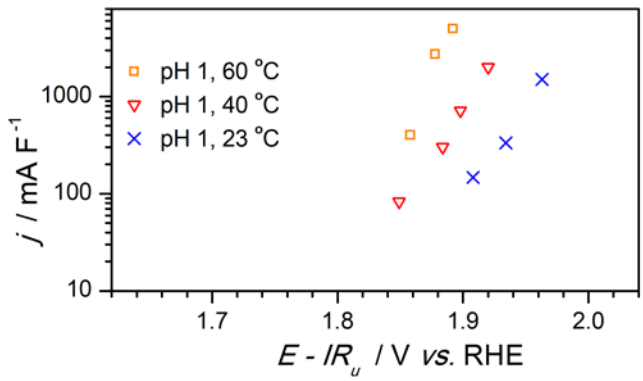

Supplementary Figure 27. Qausi-steady state polarisation plots for the oxidation of aqueous 1 M H_2SO_4 containing 5 mM Co^{2+}, 1 mM Fe^{3+} and 0.5 mM Pb^{2+} with Pt/Ti electrodes at different temperatures. Data were derived from galvanostatic experiments and corrected for IR_u drop. Currents are normalised to the capacitances of electrodes measured by cyclic voltammetry post-testing (see Supplementary Figure 26).

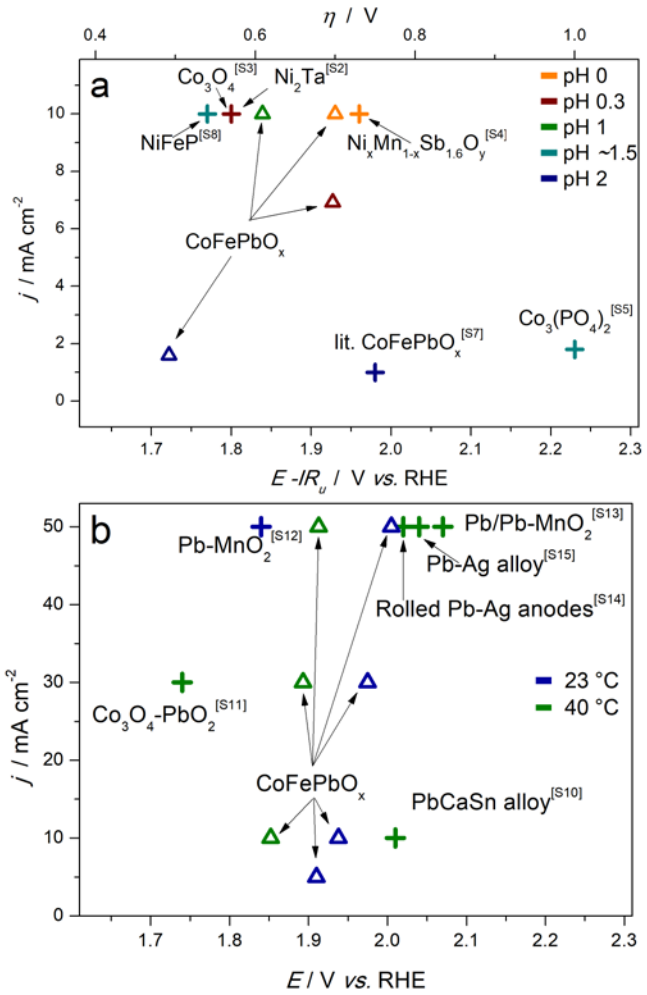

Supplementary Figure 28. Comparison of the reported performances at low pH of the OER catalysts designed for (a) water splitting and (b) electrowinning with the performance of the *in situ* generated $CoFePbO_x$ system. In panel (a), all data are at ambient temperature (23 °C for the present work and 23-25 °C for literature reports) and colour-coded according to pH; potentials are corrected for ohmic losses. In panel (b), data are colour-coded according to temperature and potentials are not corrected for ohmic losses for both $CoFePbO_x$ and literature sources, since the latter do not report the R_u data; 1 M H_2SO_4 was used for $CoFePbO_x$, while conditions used for the literature catalysts are provided in Supplementary Table 6.

Supplementary Table 6. Performance of the selected OER catalysts designed for the operation at low pH.

Catalyst (Substrate)	Electrolyte	E (V *vs.* RHE) / j (mA cm^{-2})	T (°C)	Stability	Ref.
Water-splitting systems [a]					
Ni_2Ta (Sn-Cu wire)	0.5 M H_2SO_4	1.8 V / 10 mA cm^{-2}	23	not available	2
Co_3O_4 (FTO)	0.5 M H_2SO_4	1.8 V / 10 mA cm^{-2}	23	12 h	3
$Ni_xMn_{1-x}Sb_{1.6}O_y$ (ATO)	1 M H_2SO_4	1.97 V / 10 mA cm^{-2}	23	168 h	4
$Co_3(PO_4)_2$ (ITO)	1 M H_3PO_4 (pH 1.6)	2.3 V / 1.8 mA cm^{-2}	23	30 h	5
$IrO_x/SrIrO_3$ ($SrTiO_3$)	0.5 M H_2SO_4	1.52 V / 10 mA cm^{-2}	23	30 h	6
$CoFePbO_x$ (FTO)	0.5 M Na_2SO_4 (pH 2)	1.98 V / 1 mA cm^{-2}	23	50 h	7
Ba[Co-POM] (Carbon paper)	1 M H_2SO_4	1.73 V / 10 mA cm^{-2}	23	not available	8
NiFeP	0.05 M H_2SO_4	1.76 V / 10 mA cm^{-2}	23	30 h	9
Lead-based systems for electrowinning [b]					
PbCaSn alloy	1.83 M H_2SO_4 (pH -0.26)	2.01 V / 10 mA cm^{-2}	35	0.25 h	10
PbO_2-Co_3O_4 (Ti-SnO_2-Sb_2O_3)	1.83 M H_2SO_4 (pH -0.26)	1.74 V / 30 mA cm^{-2}	40	168 h	11
Pb-MnO_2	1.63 M H_2SO_4 (pH -0.21)	1.84 V / 50 mA cm^{-2}	25	72 h	12
Pb/Pb-MnO_2 composite	1.63 M H_2SO_4 (pH -0.21)	2.07 V / 50 mA cm^{-2}	35	72 h	13
Rolled Pb-Ag anodes	1.52 M H_2SO_4 (pH -0.18)	2.02 V / 50 mA cm^{-2}	35	15 days	14
Commercial Pb-Ag alloy	1.83 M H_2SO_4 (pH -0.26)	2.04 V / 50 mA cm^{-2}	38	24 h	15

[a] Potentials are corrected for iR_u-drop. [b] Potentials are not corrected for ohmic losses, since R_u values were not reported in these publications.

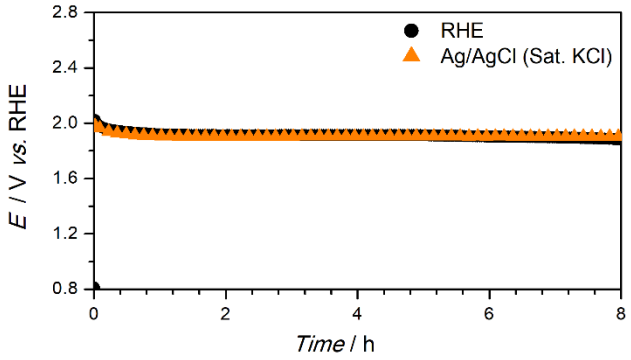

Supplementary Figure 29. Galvanostatic oxidation (operating current density of 100 mA cm^{-2}) of aqueous 1 M H_2SO_4 solutions containing 5 mM Co^{2+}, 1 mM Fe^{3+} and 0.5 mM Pb^{2+} at 60 °C with Pt/Ti electrodes using homemade RHE (*black*) and Ag|AgCl|KCl_{sat} (*orange*) reference electrodes. Potentials are not corrected for ohmic losses.

SUPPLEMENTARY REFERENCES

1. Lide, D. R., CRC Handbook of Chemistry and Physics, 84th Edition, CRC Press, (2003-2004).
2. Mondschein, J. S. *et al.* Intermetallic Ni_2Ta Electrocatalyst for the Oxygen Evolution Reaction in Highly Acidic Electrolytes. *Inorg. Chem.* **57,** 6010–6015 (2018).
3. Mondschein, J. S. *et al.* Crystalline Cobalt Oxide Films for Sustained Electrocatalytic Oxygen Evolution under Strongly Acidic Conditions. *Chem. Mater.* **29,** 950–957 (2017).
4. Moreno-Hernandez, I. A. *et al.* Crystalline nickel manganese antimonate as a stable water-oxidation catalyst in aqueous 1.0 M H_2SO_4. *Energy Environ. Sci.* **10,** 2103–2108 (2017).
5. Bloor, L. G., Molina, P. I., Symes, M. D. & Cronin, L. Low pH electrolytic water splitting using earth-abundant metastable catalysts that self-assemble in situ. *J. Am. Chem. Soc.* **136,** 3304–3311 (2014).
6. Staszak-Jirkovský, J. *et al.* A highly active and stable $IrO_x/SrIrO_3$ catalyst for the oxygen evolution reaction. *Science* **353,** 1–8 (2015).
7. Huynh, M., Ozel, T., Liu, C., Lau, E. C. & Nocera, D. G. Design of template-stabilized active and earth-abundant oxygen evolution catalysts in acid. *Chem. Sci.* **8,** 4779–4794 (2017).
8. Blasco-Ahicart, M., Soriano-Lopez, J., Carbo, J. J., Poblet, J. M. & Galan-Mascaros, J. R. Polyoxometalate electrocatalysts based on earthabundant metals for efficient water oxidation in acidic media. *Nat. Chem.* **10,** 24–30 (2018).
9. Hu, F. *et al.* Amorphous Metallic NiFeP: A Conductive Bulk Material Achieving High Activity for Oxygen Evolution Reaction in Both Alkaline and Acidic Media. *Adv. Mater.* **29,** 1–9 (2017).
10. Yu, P. & Keefe, T. J. O. Evaluation of Lead Anode Reactions in Acid Sulfate Electrolytes. *J. Electrochem. Soc.* **149,** A558–A569 (2002).
11. Nikoloski, A. N. & Barmi, M. J. Novel lead-cobalt composite anodes for copper electrowinning. *Hydrometallurgy* **137,** 45–52 (2013).
12. Ma, R. *et al.* Oxygen evolution and corrosion behavior of low-MnO_2-content Pb-MnO_2 composite anodes for metal electrowinning. *Hydrometallurgy* **159,** 6–11 (2016).
13. Li, Y. *et al.* Oxygen evolution and corrosion behaviors of co-deposited Pb/Pb-MnO_2 composite anode for electrowinning of nonferrous metals. *Hydrometallurgy* **109,** 252–257 (2011).
14. Yang, H. T. *et al.* Electrochemical behavior of rolled Pb-0.8%Ag anodes. *Hydrometallurgy* **140,** 144–150 (2013).
15. Sorour, N., Su, C., Ghali, E. & Houlachi, G. Effect of ionic liquid additives on oxygen evolution reaction and corrosion behavior of Pb-Ag anode in zinc electrowinning. *Electrochim. Acta* **258,** 631–638 (2017).